Geochemistry and Evolution of the Bloodgood Canyon Tuff, Mogollon-Datil Volcanic Field, New Mexico, USA: The Evolution of Crystal Sizes in an Open Magmatic System

Missouri State University
Department of Geography, Geology and Planning

Emily Salings, Gary Michelfelder, Shannon P. Rentz
Department of Geography, Geology and Planning, Missouri State University, Springfield, MO 65897, USA
Salings145@live.missouristate.edu

Missouri State University Volcanology, Petrology and Geochemistry Research Group

Abstract & Background

The Bloodgood Canyon tuff is a rhyolitic ignimbrite erupted at 28 Ma in southwestern New Mexico, USA. Three samples representing the stratigraphic section were studied in an effort to better understand the pre- and syn-eruptive history of the magma storage system and place constraints on the timescales of its existence. The samples contain phenocrysts of K-spar>Plag>Quartz>Biotite>Titanite, few lithic fragments, and pumice. Here we present bulk-rock geochemistry and crystal size distributions (CSDs) for crystals ranging from ~10 to 2000 μm for three mineral phases: plagioclase, quartz and K-feldspar.

Quartz phenocrysts are usually euhedral but may be broken up or resorbed. Phenocrysts of quartz are typically smaller than the K-feldspars that frequent the samples (~100 μm versus 1000-2000 μm K-feldspars). The CSD slope for this population is a linear trend that steepens until it nears the 1000 μm scale. The plagioclase phenocrysts occur in two phases: one as larger, sieved and resorbed phenocrysts, and second as smaller euhedral twinned phenocrysts. The CSD slope for plagioclase is a concave up trend, with few phenocrysts between 100 and 1000 μm, and a higher population of <100 μm phenocrysts than >1000 μm. K-feldspar phenocrysts are typically sanidine and occur as large, sieved phenocrysts, large, unsieved phenocrysts, or small, non-twinned euhedral phenocrysts. It is very uncommon to see a twinned K-feldspar phenocryst in these samples. The CSD slope for K-feldspar is a parabola because of the equal distribution of <100 μm and >1000 μm phenocrysts.

We interpret these crystal populations as resulting from a shift in crystallization regime. We suggest that the CSD slopes describe a pre-eruptive quartz + K-feldspar growth dominated regime and a plagioclase unstable regime. This was followed by a population that grew during nucleation at the onset of decompression at the initiation of eruption represented by the steeper slope. Initial crystal growth may coincide with eruption and collapse of the Gila Cliff Dwellings caldera 4 million years before the eruption of the BCT as indicated by the larger resolved crystal phases. Remobilization of the magma mush may have destabilized the magma chamber and allowed new phenocryst populations to grow for thousands of years before eruption.

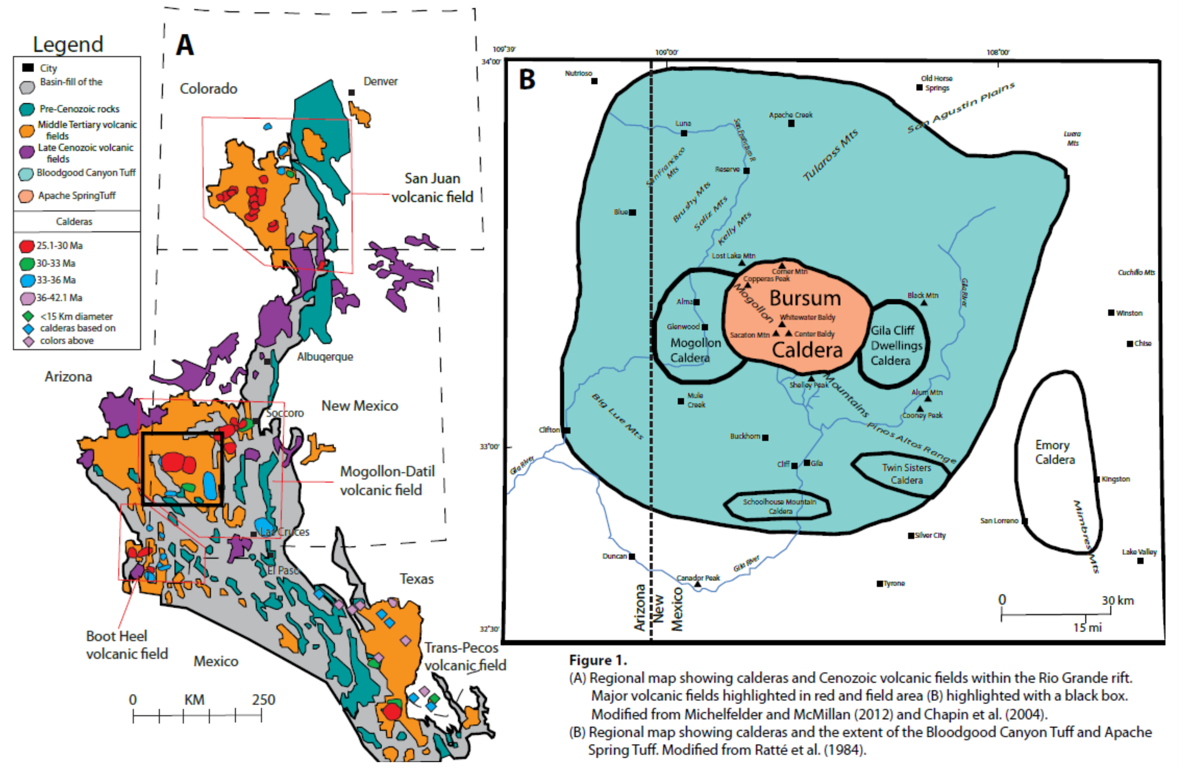

Figure 1.
(A) Regional map showing calderas and Cenozoic volcanic fields within the Rio Grande rift. Major volcanic fields highlighted in red and field area (B) highlighted with a black box. Modified from Michelfelder and McMillan (2012) and Chapin et al. (2004).
(B) Regional map showing calderas and the extent of the Bloodgood Canyon Tuff and Apache Spring Tuff. Modified from Ratté et al. (1984).

(Below) Figure 2.
Regional tectonic processes in New Mexico.
(A) Farallon plate is subducting beneath the North American plate
(B) Farallon plate begins to bend, allowing magma to upwell
(C) Farallon plate breaks, allowing mantle material to upwell into the upper crust, rifting thins the crust
(D) Mantle material causes crustal magma chambers to mobilize and erupt
(E) No magmatism as crust continues to thin from rifting
(F) Rifting causes more mantle-derived basaltic eruptions

From McMillan et al. (2000).

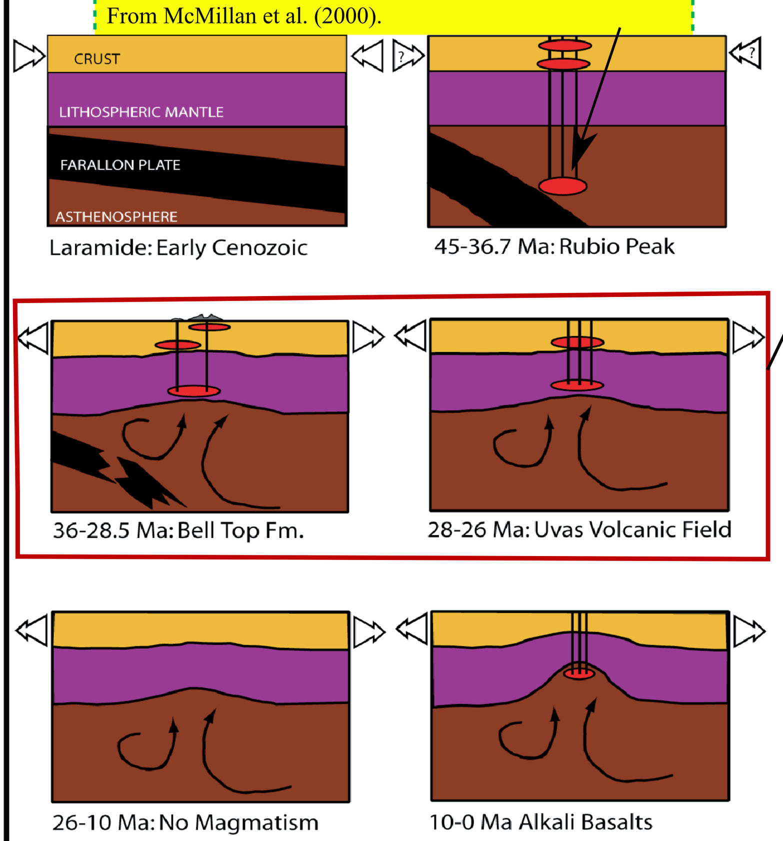

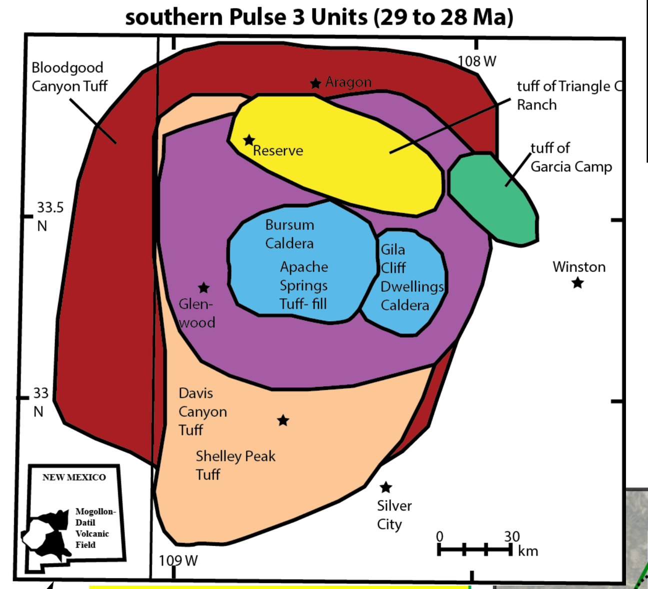

(above) Figure 3.
Extent map of various tuffs erupted from 29-28 Ma.

This study will focus on the Bloodgood Canyon Tuff in addition to the Apache Spring Tuff and Fanney Rhyolite. These units are associated with the Bursum caldera, which overprints the Mogollon and Gila Cliff Dwellings calderas.
Bloodgood Canyon Tuff = 28 Ma
Apache Spring Tuff = 27.9 Ma
Ages from McIntosh et al. (1990).
Redrafted from McIntosh et al. (1992).

Research Question:

What processes formed the Bloodgood Canyon Tuff?

(below) Figure 4.
Isopach map of the Bloodgood Canyon Tuff
Stratigraphic measurements were taken in the field during summer 2016. New extent shows the Bloodgood is more voluminous than previously reported. Original extent and caldera outlines from Ratté et al. (1984).

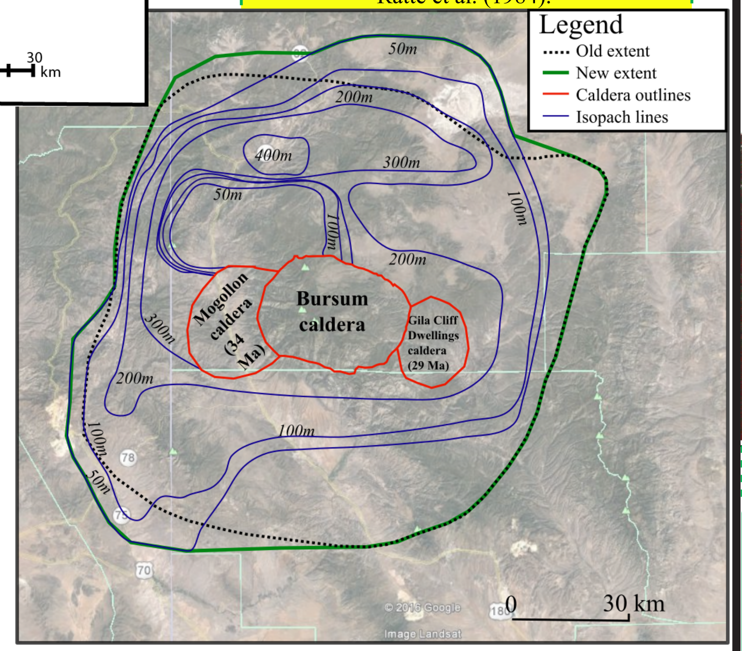

Whole-rock Geochemistry & Petrography

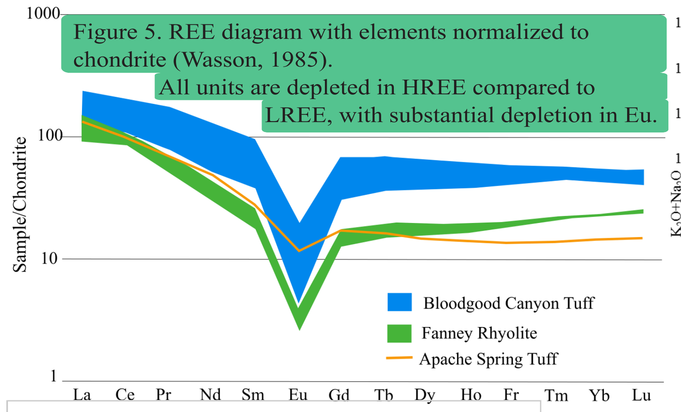

Figure 5. REE diagram with elements normalized to chondrite (Wasson, 1985).
All units are depleted in HREE compared to LREE, with substantial depletion in Eu.

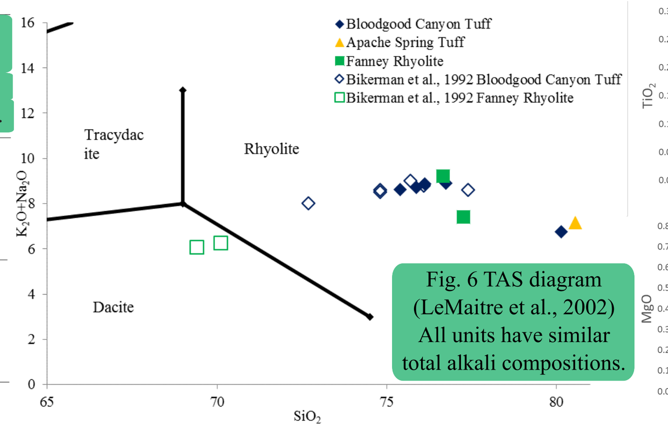

Fig. 6 TAS diagram (LeMaitre et al., 2002)
All units have similar total alkali compositions.

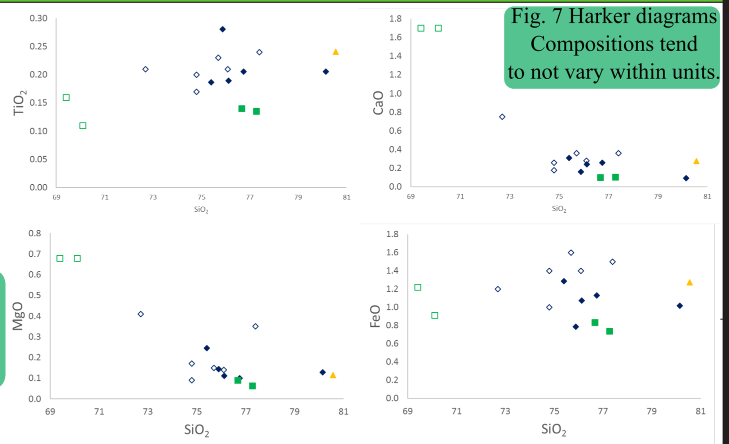

Fig. 7 Harker diagrams
Compositions tend to not vary within units.

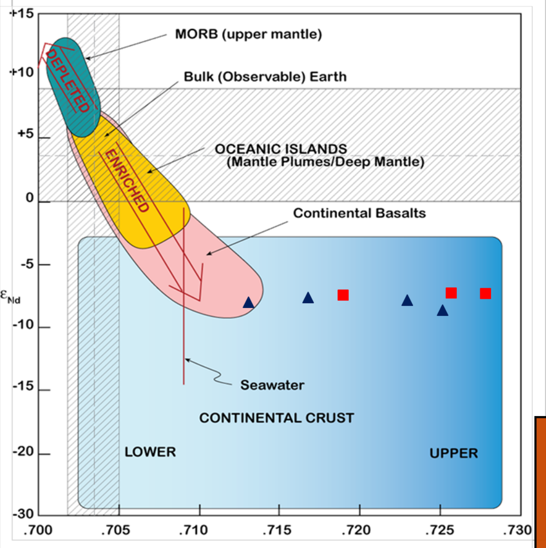

Figure 8. εNd vs. $^{87}Sr/^{86}Sr$ diagram
Blue triangles are data from Bikerman et al. (1992).
Red squares are data from this study.
$^{87}Sr/^{86}Sr$ values vary within the unit but εNd values remain the same.
Continental crust values from Rudnick and Gao (2010).

The Bloodgood Canyon Tuff
28 Ma (McIntosh et al., 1990)
Compositionally zoned
High-silica rhyolite tuff
>1000 km³ (Ratté et al., 1984)
Crystal poor to crystal rich
Large pumice fragments
Moderately to densely welded

Apache Spring Tuff
27.9 Ma (McIntosh et al., 1990)
Compositionally zoned
High-silica rhyolite tuff
>1200 km³ (Ratté et al., 1984)
Lithic-rich
Moderately to densely welded

Fanney Rhyolite
24.4 and 26.4 Ma
(Bikerman et al., 1992)
Resurgent dome and ring-intrusives
Crystal-poor
Flow-banded rhyolite

Figure 9. Stratigraphic Variations

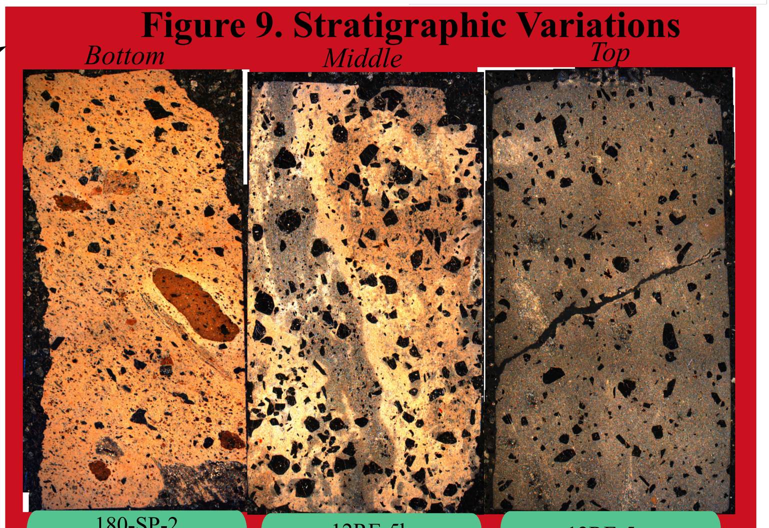

180-SP-2	12RE-5b	12RE-5a
Contains pumice, lithics, K-spar>Q>Biotite. Trace hornblende. HB, PYX in pumices. 12% crystallinity	Contains long, squished pumices, K-spar>Q>Plag>Fe-Ti oxides. 22% crystallinity	Contains pumice, K-spar>Quartz, trace hornblende. 17% crystallinity

SEM-Element maps

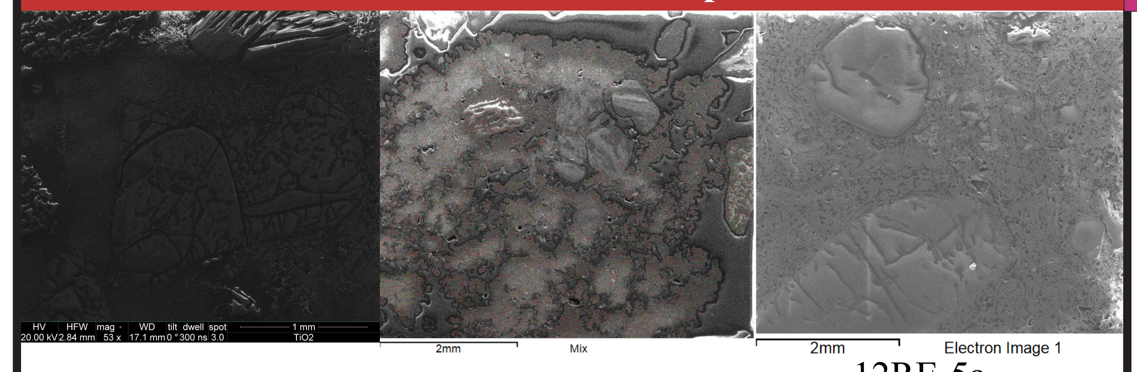

12RE-5b ETD image of Quartz phenocryst

180-SP-2 SEM image of feldspar phenocrysts

12RE-5a SEM image of felspar phenocryst (bottom) and Q phenocryst (top)

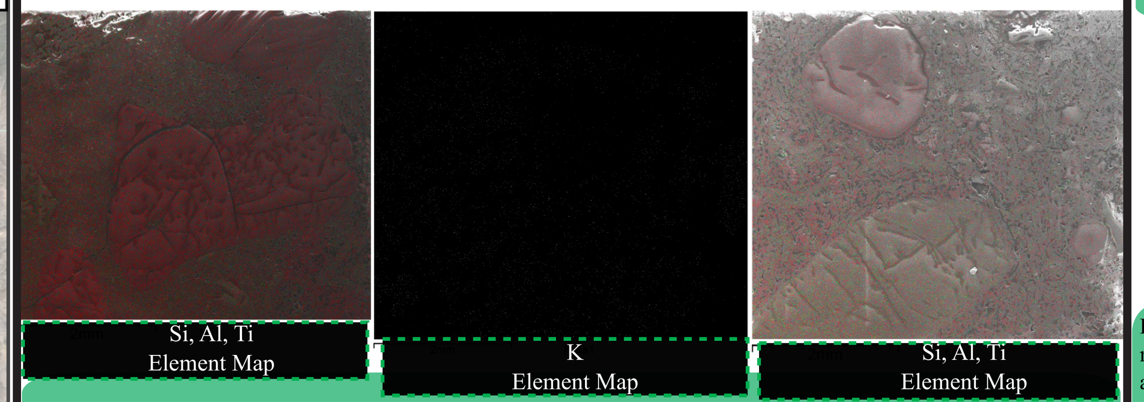

Figure 10. SEM element maps showing the concentrations of elements in specific images. Quartz grains contain mostly Si, while feldspars will contain Al, K, and Na. Element maps confirm mineral phases that are otherwise difficult to distinguish.

Modeling

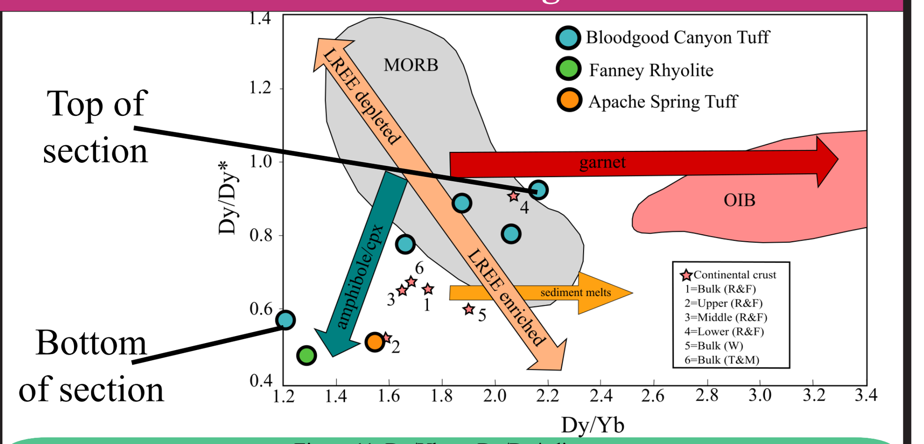

Figure 11. Dy/Yb vs. Dy/Dy* diagram
Fanney Rhyolite and Apache Spring Tuff are derived from a source that is fractionating amphibole/cpx. The Bloodgood Canyon Tuff bottom sample is in a source that is fractionating amphibole but the top of the section is from a garnet stable source.
Data added from Davidson et al. (2013).

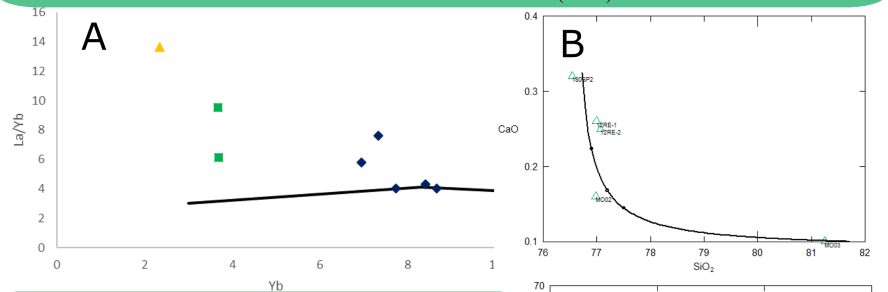

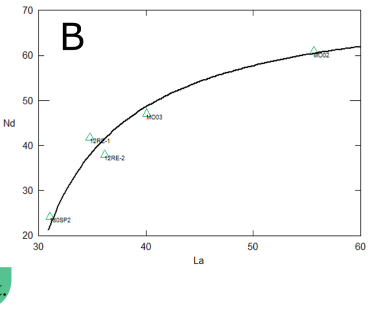

Figure 12a. Assimilation and Fractional crystallization model. Endmembers used were amphibolite (Amato et al., 2012) and the Davis Canyon Tuff (Rentz et al., 2016). While this model does not form all units of the Bloodgood, it does form one endmember of the unit (180-SP-2). Mass balanced with IgPet.
Figure 12b. Mixing model
Endmembers used were 180-SP-2 (bottom of section) and MO-03 (top of section). Mixing resulted in forming the samples of the mid-section. Mass balanced with IgPet.

Crystal Size Distributions using CSDCorrections program (Higgins, 2000)

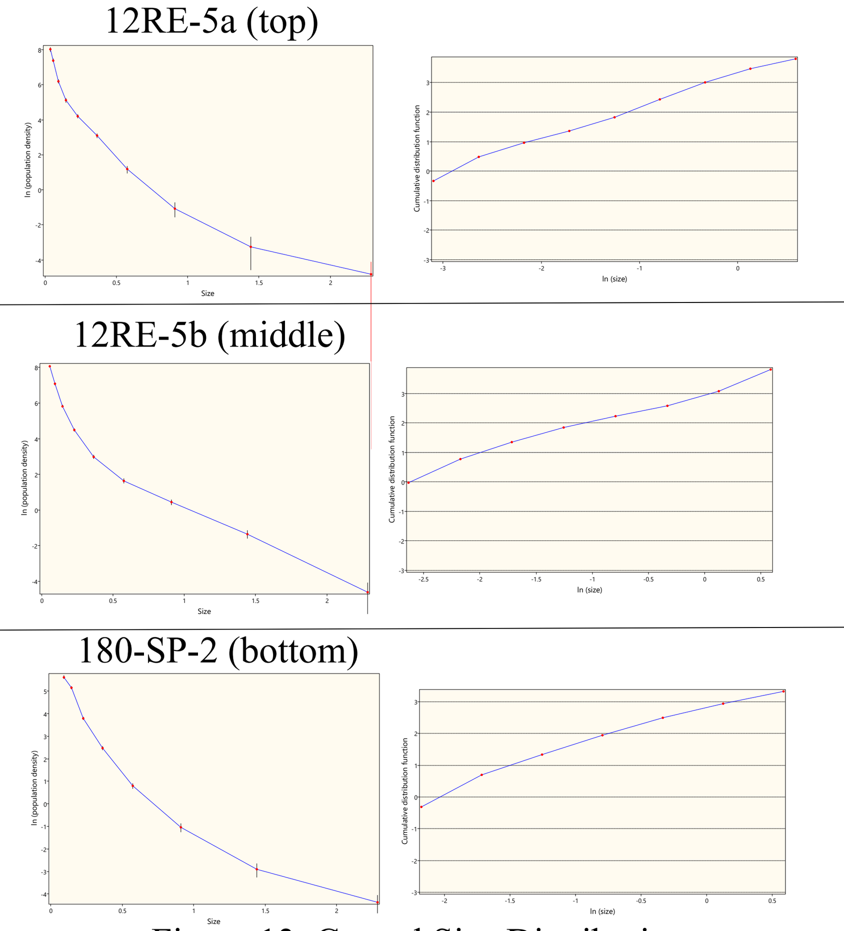

Figure 13. Crystal Size Distributions
All phases included in all diagrams

(12RE-5a) CSD curves show more frequent occurence of smaller (<0.5mm) crystals and relatively few crystals >1mm.

(12RE-5b) CSD curves show more frequent occurence of >1mm crystals than other samples, with the same distribution of <0.5mm crystals as 180-SP-2.

(180-SP-2) CSD curves show a relatively symmetrical concave pattern, but crystals >1 mm are relatively sparse.

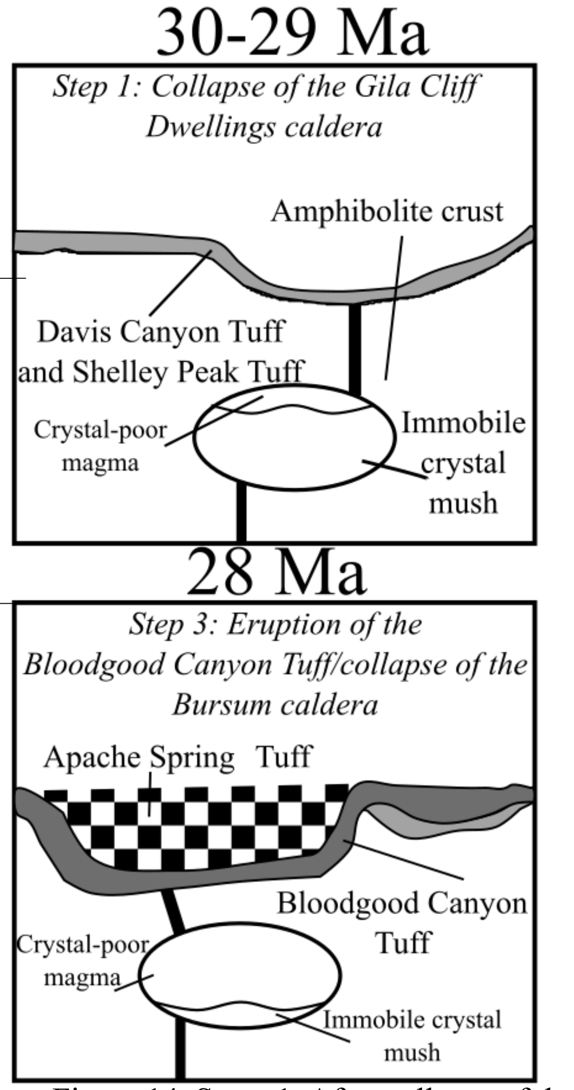

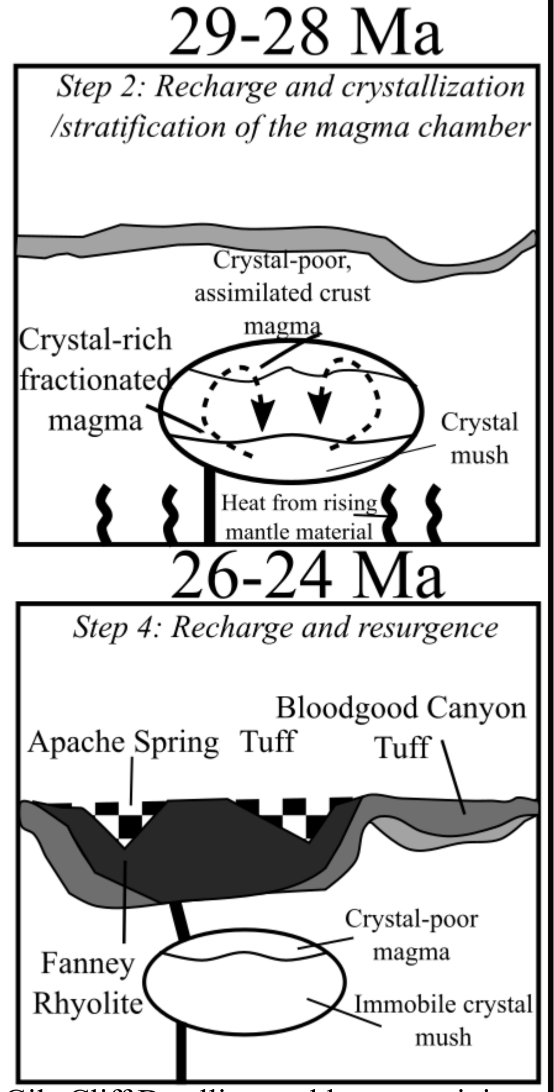

Figure 14. Stage 1: After collapse of the Gila Cliff Dwellings caldera, remaining magma assimilates with the amphibolitic-composition crust (as shown in Figure 11 and Figure 12a).
Stage 2: In the peak of the ignimbrite flare-up, ponding mafic magma remobilizes the crystal mush (Bachmann and Bergantz, 2004).
The remaining Gila Cliff Dwellings caldera magma that had assimilated with the amphibolitic-composition crust begins mixing with the remobilized crystal mush (as shown in Figure 12b).
Stage 3: The Bloodgood Canyon Tuff erupts at 28.0 Ma, erupting stratified sections of the chamber. At 27.9 Ma the Apache Spring Tuff erupts and filled in the Bursum caldera.
Stage 4: At ~26 Ma, the Fanney Rhyolite forms the resurgent dome of the Bursum caldera. Ring-fractures from the collapse are filled in with the Fanney Rhyolite and smaller pyroclastic flows.

Conclusion

The Bloodgood Canyon Tuff represents a stratified magma chamber. Existing magma from the Gila Cliff Dwellings caldera assimilated with amphibolite-composition crust. Heat from rising mafic magma during the ignimbrite flare-up remobilized the crystal mush (Bachmann and Bergantz, 2004) and allowed mixing between the melting crystal mush and the Gila-Cliff-Dwellings-magma+assimilated-amphibolitic-composition-crust magma.

Future Research

Future research will include:
(1) Mineral grain analysis within the Bloodgood Canyon Tuff using electron microprobe.
(2) Individual phase crystal size distributions
(3) Boron isotope analysis
(4) Connection between Bloodgood Canyon Tuff and the Apache Spring Tuff.

Acknowledgements

Thank you to the Missouri State University Graduate College, College of Natural and Applied Sciences, and Department of Geography, Geology, and Planning for support and grants during this project.
Thank you to the Geological Society of America for the Graduate Research Grant.
Thank you to Frank Ramos and New Mexico State University for use of the clean lab and MC-ICP-MS. Thank you to the GeoAnalytical Lab at Washington State University for XRF and ICP-MS work.

References

Amato, J. and Becker, T., 2012, Proterozoic rocks of the Caballo Mountains and Kingston Mining District: U-Pb geochronology and correlations within the Mazatal Province of southern New Mexico: New Mexico Geological Society Guidebook: Warm Springs Region, p. 227-234.
Bachmann, O. and Bergantz, G., 2004, On the Origin of Crystal-poor Rhyolites: Extracted from Batholithic Crystal Mushes: Journal of Petrology, v. 45, p. 1565-1582.
Bikerman, M., Bell, K., and Card, J., 1992, Strontium and neodymium isotopic study of the western Mogollon-Datil volcanic region, New Mexico, USA: Contributions to Mineralogy and Petrology, v. 109, p. 459-470.
Davidson, J., Turner, S., and Plank T., 2013, Dy/Dy*: Variations arising from mantle sources and petrogenic processes: Journal of Petrology, v. 54, p. 525-537.
Higgins, M.D., 2000, Measurement of Crystal Size Distributions: American Mineralogist, v. 85, p. 1105-1116.
McIntosh, W., Sutter, J., and Chapin, C., 1990, High-precision 40Ar/39Ar sanidine geochronology of ignimbrites in the Mogollon-Datil volcanic field, southwestern New Mexico: Bulletin of Volcanology, v. 52, p. 584-601.
McMillan, N.J., Dickin, A.P.; and Haag, D. 2000, Evolution of magma source regions in Rio Grande rift, Southern New Mexico: Geological Society of America Bulletin, v. 112, no. 10, p. 1582-1593.
Ratté, J., Marvin, R., Naeser, C., and Bikerman, M., 1984, Calderas and ash flow tuffs of the Mogollon Mountains, southwestern New Mexico: Journal of Geophysical Research, v. 89, p. 8713-8732.
Rudnick, R.L., and Gao, S., 2010, Composition of the Continental Crust: Readings from Treatise on Geochemistry: eds. Holland, H.D. and Turekian, K.K., p. 131-196.
Rentz, S., Michelfelder, G., and Salings, E., 2016, The Cooney Tuff: Ash fall in a calc-alkaline subduction related volcanic field, southern New Mexico: Geological Society of America Abstracts with Programs, v. 48, no. 7, doi: 10.1130/abs/2016AM-281935.